Higgs measurements in the diboson final state

Ioannis Nomidis
LPNHE-Paris / CNRS, France
on behalf of the ATLAS Collaboration

These proceedings summarise recent measurements of the Higgs boson properties using its diboson final states performed with 36.1 fb^{-1} of data collected with the ATLAS detector in 13 TeV proton-proton collisions at the LHC. Two most recent results are highlighted: the measurement of the Higgs production cross-section from gluon-gluon fusion and vector-boson-fusion modes with the $H \to WW^*$ decay and also a measurement of the Higgs boson production combining the differential cross-sections of $H \to ZZ^*$ and $H \to \gamma\gamma$ decay channels.

ATL-PHYS-PROC-2018-021
27 April 2018

1 Introduction

One of the main aspects of the ATLAS experiment[1] is to elucidate the nature of electroweak symmetry breaking. In the Standard Model (SM), the Higgs boson is responsible of such symmetry breaking and a consequence of this are precise correlations between the elementary particle masses and their coupling to the Higgs boson. Following the discovery of a Higgs boson during Run-1 of the LHC, the goal is to study its various production and decay modes and measure its couplings with high precision in order to confirm consistency with the SM predictions and constrain the allowed phase space for beyond-the-SM phenomenology. The goal in Run-2 is to exploit the increase in luminosity and center-of-mass energy and improve on the precision of the cross-section and couplings measurements with respect to Run-1.

The $H \to b\bar{b}$ decay is favoured in terms of branching ratio, but experimentally it is much more challenging to discriminate from background, making diboson decays of the Higgs boson particularly important for studies of production and couplings. The $H \to \gamma\gamma$ and $H \to ZZ^* \to 4\ell$ final states, despite the much smaller branching ratios, give clean signal mass peaks that can be fully reconstructed with high resolution from well-understood backgrounds, also in multi-jet environments. The $H \to WW^* \to \ell\ell\nu\nu$ final state has a more complex background composition but, thanks to its relatively large branching ratio, it has the potential of measurements with higher signal significance. Thanks to these features, the analyses of these diboson final states can probe all production modes in the same final state and eventually drive the overall sensitivity of the current measurements. The analysis of the $H \to \gamma\gamma$ and $H \to ZZ^* \to 4\ell$ decay channels allows also the direct measurement of the mass of the Higgs boson. In Run-2, the ATLAS collaboration has analysed 36 fb^{-1} of data collected during 2015-2016 and provided measurements of mass, fiducial, differential and total cross-sections and couplings in the four-lepton and diphoton final states[2,3,4]. In this article, two recent results using this dataset are presented: a) gluon-gluon- and vector-boson-fusion (ggF, VBF) production measurements in the $H \to WW^*$ decay,[5] and b) the combination of the $H \to \gamma\gamma$ and $H \to ZZ^* \to 4\ell$ cross-sections[6].

2 ggF and VBF production measurements in the $H \to WW^*$ decay channel

The analysis of the $H \to WW^*$ decay is performed using the leptonic decays of the W bosons, giving a signal that consists of two prompt isolated leptons with small opening angle due to their spin correlations in this decay, and also missing transverse energy from the neutrinos. These features are exploited in the event selection in order to suppress backgrounds with similar final state.

Regarding backgrounds in general, there are many processes that contribute. To evaluate the understanding of the background composition and eventually constrain the normalisation of the dominant sources, control regions (CRs) that are orthogonal to the signal region are built by relaxing/inverting the signal selections. Events with zero, one or at least two jets of

$p_{\mathrm{T}} > 30$ GeV are studied separately in order to probe the ggF and VBF production modes and also to exploit the fact that they have quite different background composition. For example, there is the non-resonant WW production that is relatively higher in events with no jets, while top quark pair production and associated top-W production become dominant in the one- and two-jet categories. Drell-Yan production of τ-lepton pairs is also contributing to the background. Background from misidentified leptons has a smaller contribution. Its contribution in the signal region is obtained with a technique that is using Z+jets data and minimum input from simulation, mainly to account for differences between Z and W+jets, which is also contributing as a process. Lastly, non-resonant production of other dibosons also contributes a small amount which is obtained from MC simulation normalised to next-to-leading-order predictions.

A few differences are pointed out in the comparison of the present analysis to the one performed in Run-1[7]. Currently only the e+μ final state is considered due to the fact that the same-flavour final states suffer from a much larger Drell-Yan background which does not allow them to improve the significance of the measurement. Also the associated production with a vector boson, having quite smaller cross-section and a lower sensitivity given the current dataset, is not included in this result. Moreover, due to the relative increase of the top background in Run-2 because its cross-section grows faster with $\sqrt{s}$ than the other processes, actions were taken to suppress the top background further in the zero-jet category. A veto on b-jets of $p_{\mathrm{T}} > 20\,\mathrm{GeV}$ is introduced together with an additional zero-jet top-enhanced CR to constrain this component.

The signal region for ggF is split into 16 categories in total and the transverse mass of the WW^* system is used as the discriminant for the Higgs boson signal. For VBF, a multivariate discriminant based on a boosted decision tree (BDT) is used instead; the signal region is split into four categories according to the BDT score. All categories are fitted simultaneously with the CRs to constrain the background normalizations. The post-fit result is shown in Figure 1 separately for the ggF- and VBF-targeted regions. In the plot of the transverse mass for events with one or zero jets, a clean signal excess with a 6.3σ significance is seen (5.2σ expected). In the VBF-targeted region with at least two jets, the signal significance observed is 1.9σ, slightly lower than the expectation of 2.7σ.

The size of the data sample in the signal region yields a 8% uncertainty on the ggF and 46% uncertainty on the VBF measurement. Regarding the systematic uncertainties entering the measurements, they are many and only a short summary is given here. The experimental ones are mostly related to the reconstruction of jets and missing transverse energy (MET). Thanks to the excellent jet and MET performance of the ATLAS detector, they are kept at remarkably low levels and sum up to about 8%–9% for both categories. Theoretical understanding of the signal and background processes in the simulation is a crucial aspect of this analysis. The nature of the uncertainty has to do with the modelling of the processes, evaluated by comparing different generators and parton showers, and with the missing higher orders that affect not only the overall normalization of the components but also the modelling of the migrations between the jet categories. The theoretical uncertanties sum up to 8% for ggF and to 21% for VBF, but given the statistical precision of the two measurements, they have a larger impact on the ggF than on the VBF one.

The measured signal strengths of ggF and VBF are $\mu_{\mathrm{ggF}} = 1.21^{+0.12}_{-0.11}(\mathrm{stat.})^{+0.18}_{-0.17}(\mathrm{syst.}) = 1.21^{+0.22}_{-0.21}$ and $\mu_{\mathrm{VBF}} = 0.62^{+0.30}_{-0.28}(\mathrm{stat.})\pm 0.22(\mathrm{syst.}) = 0.62^{+0.37}_{-0.36}$, respectively. The precision of the ggF measurement is as good or better than the Run-1 combined ATLAS+CMS measurement[8]. For VBF production, this is the most precise single-channel measurement regarding the expected uncertainty for a signal strength of one. The corresponding cross-sections-times-branching-ratio are $\sigma_{\mathrm{ggF}} \cdot \mathcal{B}_{H\to WW^*} = 12.6^{+2.3}_{-2.1}$ pb and $\sigma_{\mathrm{VBF}} \cdot \mathcal{B}_{H\to WW^*} = 0.50^{+0.30}_{-0.29}$ pb. The consistency with the SM prediction is demonstrated in Figure 2 and it is at the level of 1σ.

3 Differential production measurements in the $H \to \gamma\gamma$ and $H \to ZZ^* \to 4\ell$ decays

The ATLAS Collaboration has recently published results for the diphoton and four-lepton channels[3,4] including measurements of the fiducial and total cross-sections, as well as measurements of various interesting differential distributions (e.g. transverse momentum and rapidity of the Higgs boson, $p_{\mathrm{T}}^{\mathrm{H}}$, y^{H}, jet multiplicity, N_{jets}, leading jet transverse momentum, $p_{\mathrm{T}}^{\mathrm{j1}}$). The fiducial measurements are given in the phase space that is directly accessible with the ATLAS detector and with minimal assumptions on the properties of the Higgs boson. The signal composition is assumed to be that of the SM; nevertheless, the model-dependence systematic uncertainty is found to be minimal or insignificant. The fiducial measurements, exclusive in the decay (they include the branching ratio) and inclusive in the production, provide the means for a comparison with theory predictions in a model-independent manner. The measurements in both decay channels and also the differential distributions that are studied are in good agreement with the SM predictions. It is clear, however, that the precision of the theory calculations is better than the experimental one, so these comparisons will become more interesting with more data.

In anticipation of larger datasets, the combination of the available four-lepton and diphoton measurements is exercised in order to increase the sensitivity of the tests. In this combination, the branching ratios for the $H \to \gamma\gamma$ and $H \to ZZ^*$ decays of a SM Higgs boson of 125.09 GeV[9] are assumed. Acceptance corrections to extrapolate the measurements from the fiducial volume to the common, full phase space is also required. They are calculated with Monte Carlo simulated events generated with next-to-next-to-leading-order precision for ggF and next-to-next-to-leading-order precision for VBF and the other production modes. The acceptance corrections are about 50% and 42% for the diphoton and four-lepton channels, respectively, and vary mildly as a function of the observables. The measured total cross-section from the combination of the two decay channels is $57.0^{+6.0}_{-5.9}(\mathrm{stat.})^{+4.0}_{-3.3}(\mathrm{syst.})$ pb, in excellent agreement with the best available prediction of 55.0 ± 2.5 pb[10].

In the following, the differential measurements between the two channels are compared and, eventually, combined. The four aforementioned observables are considered, $p_{\mathrm{T}}^{\mathrm{H}}$, y^{H}, N_{jets} and $p_{\mathrm{T}}^{\mathrm{j1}}$. The p-value of the compatibility between the two channels in all bins of the observables considered is found to be better than 40% in all cases. The individual differential measurements from diphotons and four-leptons can be seen in Figure 3 together with their combination. The statistical uncertainty ranges from 20 to 30% and dominates the total uncertainty. The systematic uncertainty from luminosity determination is 4% and found to be among the larger ones. For the jet-based observables, jet experimental uncertainties are relatively small, typically 3%–6% and only become slightly larger than 10% in the bin with at least 3 jets, but still small in comparison with the corresponding statistical uncertainty of about 30%. The level of compatibility with various theory predictions is also evaluated with the p-value, taking into account only the uncertainties of the measurements and neglecting the uncertainties of the predictions. Generally, high level of compatibility is seen, 20% and higher. A mild excess is seen at high values of $p_{\mathrm{T}}^{\mathrm{H}}$, $p_{\mathrm{T}}^{\mathrm{j1}}$ and N_{jets}which yields lower p-values (5% in the worst case). The excess is seen for both channels but it is still within expectations from statistical fluctuations.

4 Summary

With the first 36.1 fb^{-1} of data collected in Run-2 of the LHC, ATLAS has performed measurements of the Higgs boson cross-sections and couplings that already improve on the precision achieved in Run-1. These proceedings focus on the results of two recent measurements with diboson decays.

Firstly, a measurement of the ggF and VBF production in the $H \to WW^*$ decay was presented, which improves on previous measurements in the $H \to WW^*$ decay and also yields the most precise measurement of VBF production in a single channel. The results are in very good agreement with the SM prediction. Also presented is the combination of the $H \to ZZ^* \to$

4ℓ and $H \to \gamma\gamma$ decay channels for the measurement of not only the total, but also of the differential cross-sections for a few interesting observables. This allows comparisons against theory predictions with increased precision with respect to the measurements in the individual channels. No significant deviations from the SM predictions are seen. Nevertheless, given the current statistical limitations, it is clear that these comparisons will become more interesting with more data.

These results, together with those from fermionic decays (i.e $H \to b\bar{b}$), set the foundation on which the ATLAS Collaboration will perform the conclusive measurements with the full Run-2 dataset. Irrespectively of the outcome, measurements of the Higgs properties are a major legacy.

Acknowledgements

The author is supported by the French National Research Agency (ANR) under the grant PhotonPortal.

References

1. ATLAS Collaboration, 2008 JINST 3 S08003.
2. ATLAS Collaboration, ATLAS-CONF-2017-046, http://cdsweb.cern.ch/record/2273853
3. ATLAS Collaboration, arXiv:1802.04146 [hep-ex].
4. ATLAS Collaboration, JHEP **10** (2017) 132.
5. ATLAS Collaboration, ATLAS-CONF-2018-004, http://cdsweb.cern.ch/record/2308392.
6. ATLAS Collaboration, ATLAS-CONF-2018-002, http://cdsweb.cern.ch/record/2308390.
7. ATLAS Collaboration, Phys. Rev. D **92**, 012006 (2015)
8. ATLAS and CMS Collaborations, JHEP **08** (2016) 045
9. ATLAS and CMS Collaborations, Phys. Rev. Lett. **114** (2015) 191803.
10. LHC Higgs Cross Section Working Group, D. de Florian et al., arXiv: 1610.07922 [hep-ph].

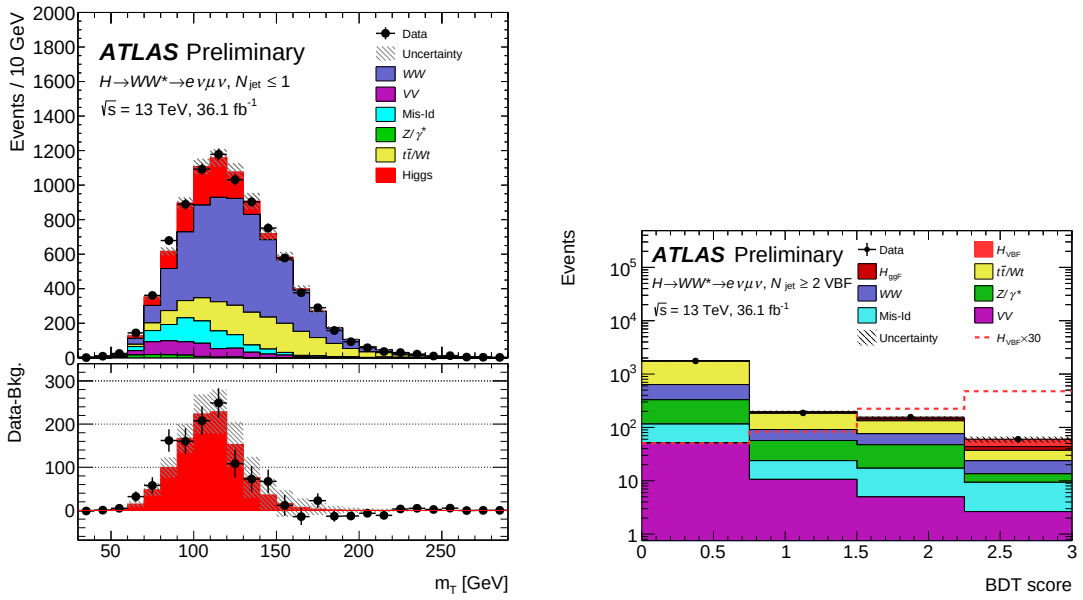

(a) (b)

Figure 1: Post-fit distribution of (a) the transverse mass for $H \to WW^*$ candidate events with less than two jets and (b) the BDT score for events with at least two jets [5]. The SM Higgs boson signal prediction shown is summed over all production processes. The bottom pad in the transverse mass figure shows the residuals of the data with respect to the estimated background compared to the distribution for a SM Higgs boson of mass 125 GeV. The background and signal processes are normalised to the result of the statistical analysis. The hatched band shows the sum in quadrature of statistical and systematic uncertainties of the signal and background predictions taking into account the pulls and data-constraints of the nuisance parameters, and the correlations between the fit regions.

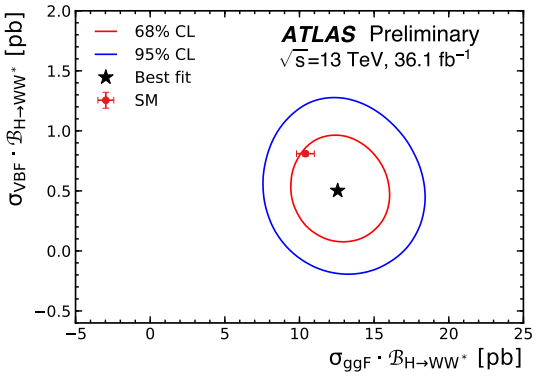

Figure 2: Best-fit value (star) and two-dimensional likelihood contours (lines) for the 68% and 95% confidence levels on $\sigma_{\mathrm{ggF}} \cdot \mathcal{B}_{H\to WW^*}$ vs. $\sigma_{\mathrm{VBF}} \cdot \mathcal{B}_{H\to WW^*}$ [5]. The SM prediction is shown with a red circle.

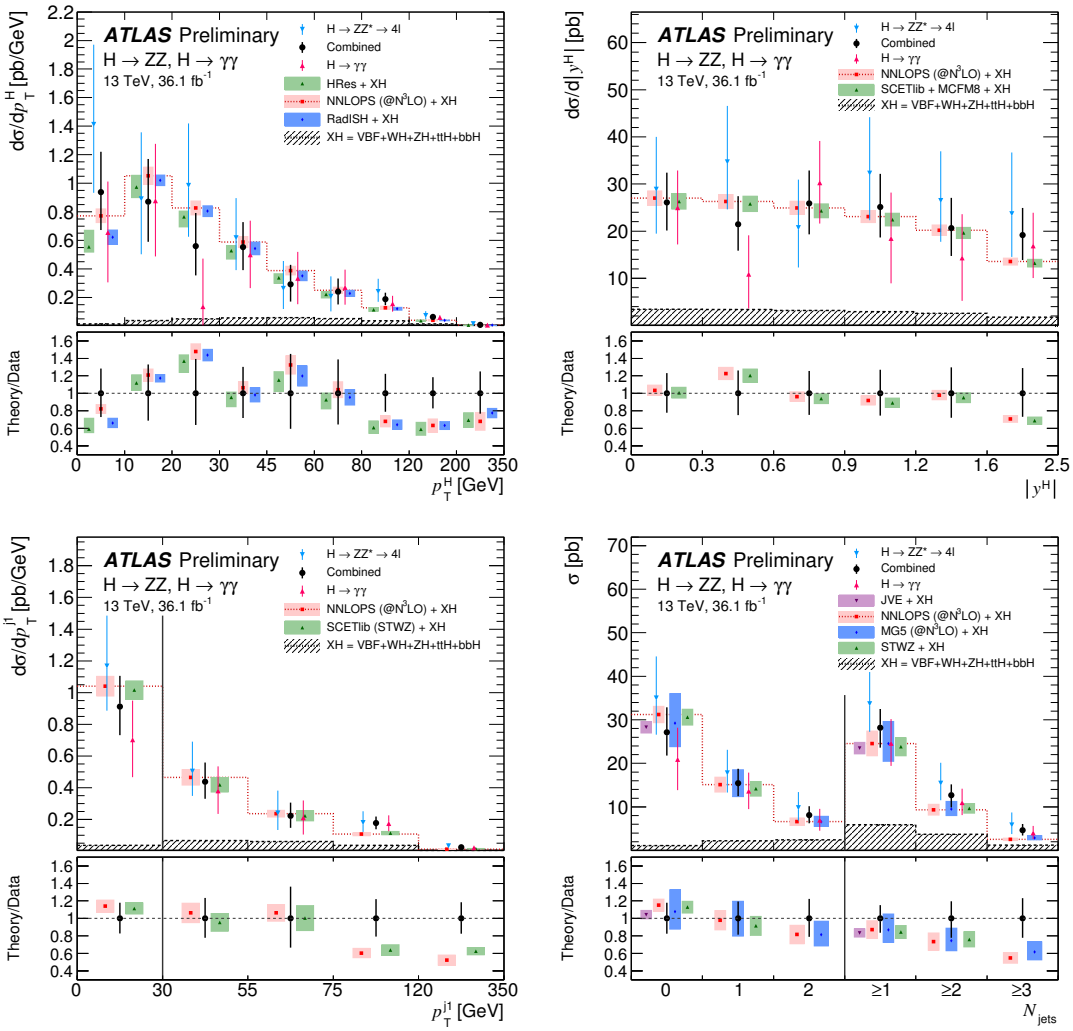

Figure 3: Differential cross-sections measured in the $H \to \gamma\gamma$ (red upward triangle) and $H \to ZZ^* \to 4\ell$ (blue downward triangle) decay channels, as well as the combined measurement (black circle) for kinematic observables of the Higgs boson and associated jets [6]. The jet multiplicity is given for jets of at least 30 GeV of transverse momentum. The first bin in the $p_{\mathrm{T}}^{\mathrm{j1}}$ distribution separated with vertical line corresponds to the zero-jet bin of the N_{jets} distribution. For comparison, various theoretical predictions are overlayed with the corresponding uncertainties from parton-distribution functions and missing higher orders. The dotted red line corresponds to the prediction obtained using NNLOPS for ggF, scaled to the N^{3}LO cross-section. Its compatibility with the data (neglecting the uncertainty of the theoretical calculations) is 29% for $p_{\mathrm{T}}^{\mathrm{H}}$, 92% for y^{H}, 45% for N_{jets} and 5% for $p_{\mathrm{T}}^{\mathrm{j1}}$. In the N_{jets} distribution plot, the MadGraph5_aMC@NLO prediction is also scaled to the N^{3}LO cross-section. Predictions for the other production processes XH are added to the ggF predictions, and also shown separately with the dashed-line histogram. For better visibility, all bins are presented in the same size, independent of their numerical width.